minerals

MDPI

Article

Hydrogen Chloride and Sulfur Dioxide Gas Evolutions from the Reaction between Mg Sulfate and NaCl: Implications for the Sample Analysis at the Mars Instrument in Gale Crater, Mars

Joanna V. Clark [1,*], Brad Sutter [2], Amy C. McAdam [3], Christine A. Knudson [3,4,5], Patrick Casbeer [2], Valerie M. Tu [2], Elizabeth B. Rampe [6], Douglas W. Ming [6], Paul D. Archer [2], Paul R. Mahaffy [3] and Charles Malespin [3]

1 Geocontrols Systems—Jacobs JETSII Contract, NASA Johnson Space Center, Houston, TX 77058, USA
2 Jacobs, NASA Johnson Space Center, Houston, TX 77058, USA
3 NASA Goddard Space Flight Center, Greenbelt, MD 20771, USA
4 University of Maryland, College Park, MD 20742, USA
5 CRESST II, Greenbelt, MD 20771, USA
6 NASA Johnson Space Center, Houston, TX 77058, USA
* Correspondence: joanna.v.clark@nasa.gov

Abstract: The Sample Analysis at Mars-Evolved Gas Analyzer (SAM-EGA) on the *Curiosity* rover detected hydrogen chloride (HCl) and sulfur dioxide (SO_2) gas evolutions above 600 °C and 700 °C, respectively, from several drilled rock and soil samples collected in Gale crater, which have been attributed to NaCl and Mg sulfates. Although NaCl and Mg sulfates do not evolve HCl or SO_2 within the SAM temperature range (<~870 °C) when analyzed individually, they may evolve these gases at <870 °C and become detectable by SAM-EGA when mixed. This work aims to determine how Mg sulfate and NaCl interact during heating and how that affects evolved HCl and SO_2 detection temperatures in SAM-EGA. Solid mixtures of NaCl and kieserite were analyzed using a thermogravimeter/differential scanning calorimeter furnace connected to a quadrupole mass spectrometer, configured to operate under similar conditions as SAM, and using X-ray diffraction of heated powders. NaCl analyzed individually did not evolve HCl; however, NaCl/kieserite mixtures evolved HCl releases with peaks above 600 °C. The results suggested that kieserite influenced HCl production from NaCl via two mechanisms: (1) kieserite depressed the melting point of NaCl, making it more reactive with evolved water; and (2) SO_2 from kieserite decomposition reacted with NaCl and water (i.e., Hargreaves reaction). Additionally, NaCl catalyzed the thermal decomposition of kieserite, such that the evolved SO_2 was within the SAM-EGA temperature range. The results demonstrated that SAM-EGA can detect chlorides and Mg sulfates when mixed due to interactions during heating. These phases can provide information on past climate and mineral formation conditions.

Keywords: Sample Analysis at Mars; *Curiosity* rover; Gale crater; chlorides; sulfates

check for updates

Citation: Clark, J.V.; Sutter, B.; McAdam, A.C.; Knudson, C.A.; Casbeer, P.; Tu, V.M.; Rampe, E.B.; Ming, D.W.; Archer, P.D.; Mahaffy, P.R.; et al. Hydrogen Chloride and Sulfur Dioxide Gas Evolutions from the Reaction between Mg Sulfate and NaCl: Implications for the Sample Analysis at the Mars Instrument in Gale Crater, Mars. *Minerals* **2024**, *14*, 218. https://doi.org/10.3390/min14030218

Academic Editors: Theodore J. Bornhorst and Kattathu Mathew

Received: 25 January 2024
Accepted: 16 February 2024
Published: 21 February 2024

Copyright: © 2024 by the authors. Licensee MDPI, Basel, Switzerland. This article is an open access article distributed under the terms and conditions of the Creative Commons Attribution (CC BY) license (https://creativecommons.org/licenses/by/4.0/).

1. Introduction

Chlorides and Mg sulfates provide important information about past climate, environmental conditions during secondary mineral formation, the chemistry of formation waters, and the preservation potential of organic materials, e.g., [1–6]. The in situ detection of these minerals is especially important for ground-truthing the presence of Mg sulfates in the Layered Sulfate-bearing unit (LSu), a hundreds-of-meters-thick unit exposed at the surface in Gale crater that has signatures of hydrated Mg sulfates detected in orbital near-infrared reflectance data [1–5]. A leading hypothesis for the deposition of LSu rocks stratigraphically above phyllosilicate-rich rocks was a change from a wet and warm climate to a cold and arid climate [1], conducive to the formation of evaporites (e.g., sulfates and chlorides). This hypothesis would be supported by the in situ detection of Mg sulfates and chlorides in laterally extensive layers. Alternatively, the detection of chlorides and

Mg sulfate in rocks with abundant veins and nodules would suggest that they formed through diagenetic processes (e.g., leaching/reprecipitation, acid-sulfate weathering) and can provide constraints on environmental conditions during secondary mineral formation such as relative humidity, temperature, and pH [6–9].

The Sample Analysis at Mars-Evolved Gas Analyzer (SAM-EGA) on the Mars Science Laboratory (MSL) *Curiosity* rover is essential for studying chlorides and Mg sulfates in Gale crater rocks when they are undetectable by other rover instruments due to factors such as poor crystallinity or low abundances. Previous work has shown that high-temperature (above 600 °C) hydrogen chloride (HCl) gas releases observed in SAM-EGA data were caused by reactions between chlorides and phases that evolve water during heating (e.g., phyllosilicates) [10]. However, it is not fully understood how other phases present in Gale crater rocks (e.g., sulfates) interact with chlorides during heating and how they affect HCl evolutions. Additionally, Mg sulfates thermally decompose and evolve sulfur dioxide (SO_2) above the temperature range of SAM, but previous work has suggested that other phases present in Gale crater samples (e.g., perchlorates) may catalyze Mg sulfate thermal decomposition to lower temperatures so that SO_2 releases are detectable by SAM-EGA [11]. The goal of this work was to determine if mixtures of $MgSO_4$ and NaCl produced distinct HCl and SO_2 evolutions that could aid in their detection in samples previously analyzed by SAM-EGA and in samples that will be analyzed in the LSu.

1.1. Background

1.1.1. SAM Instrument Overview

The SAM instrument onboard the *Curiosity* rover analyzes gases evolved during the heating of drilled rock or scooped sediment to characterize the isotopic and chemical composition of volatile-bearing phases [12]. Sample fines from unconsolidated sediment or drilled rock samples were delivered to sample cups inside SAM's Sample Manipulation System (SMS). The sample cups were transferred into one of the SAM ovens and heated from 35 to ~870 °C (35 °C/min) in He carrier gas [13]. The evolved gases (e.g., SO_2, O_2, H_2O, and HCl) from volatile-bearing phases (e.g., sulfates, phyllosilicates, and perchlorates) were then analyzed by the quadrupole mass spectrometer (QMS). The evolved gases were subsequently analyzed by gas chromatography mass spectrometry (GCMS) or the tunable laser spectrometer (TLS) [12,14,15]. This study focused on results from SAM's evolved gas analysis (SAM-EGA) mode, which examined evolved gases detected only by the QMS.

1.1.2. Gale Crater Samples

This paper includes a discussion of 25 drilled rock and scooped sediment samples collected from the Yellowknife Bay Formation to the Glen Torridon trough in the Carolyn Shoemaker Formation (Figure 1). Drilled rock and scooped sediment samples occurred over a traverse distance of over 23 km and an elevation change of over 400 m. The lithology of drilled rock samples in Gale crater reflected a fluvio-lacustrine or ancient eolian origin (Table 1 and references therein), and the scooped samples were collected from active or inactive modern eolian deposits [16–18]. Chemistry and Mineralogy (CheMin) X-ray diffraction (XRD) instrument data showed that all samples, with the exception of Edinburg, contained crystalline Ca and/or Fe sulfates (Table 1) and one sample contained halite (NaCl) at abundances above CheMin's detection limit (~1–2 wt.%) [19].

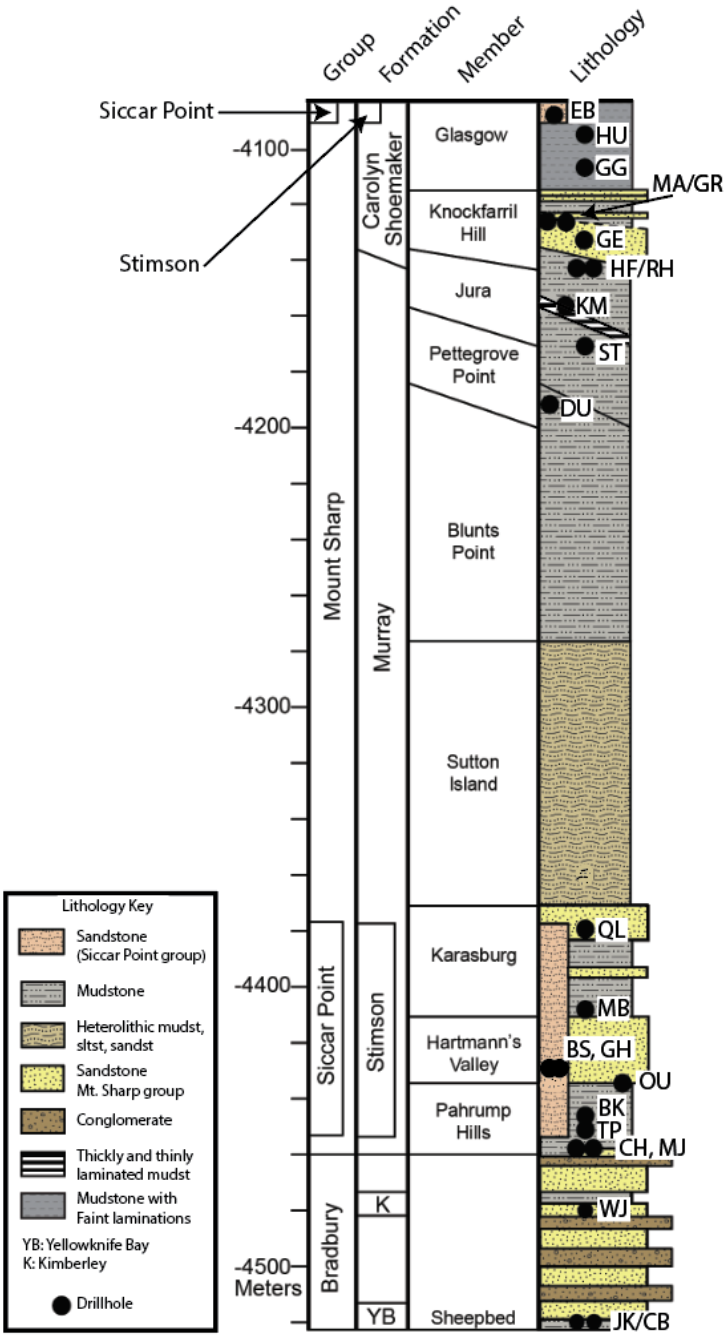


Figure 1. Stratigraphic column showing the approximate elevation of the drill samples analyzed by SAM: John Klein (JK); Cumberland (CB); Windjana (WJ); Confidence Hills (CH); Mojave (MJ); Telegraph Peak (TP); Buckskin (BK); Oudam (OU); Big Sky (BS); Greenhorn (GH); Marimba (MB); Quela (QL); Duluth (DU); Stoer (ST); Kilmarie (KM); Highfield (HF); Rock Hall (RH); Glen Etive (GE); Mary Anning (MA); Groken (GR); Glasgow (GG); Hutton (HU); and Edinburgh (EB). The scooped samples Rocknest, Gobabeb, and Ogunquit Beach are not shown. The stratigraphic column was adapted from [20].

Table 1. Samples analyzed by the SAM instrument, their primary lithology, the interpreted environment of formation, and crystalline sulfates detected by the CheMin instrument. The scooped samples are shown on the top, and the drilled-rock samples are displayed in the order that they were analyzed.

Sample	Primary Lithology	Sulfates Detected by CheMin
Rocknest (RN)	Modern eolian sediment	Anhydrite [16]
Gobabeb (GB)	Modern eolian sediment	Anhydrite [16]
Ogunquit Beach (OG)	Modern eolian sediment	Anhydrite [18]
John Klein (JK)	Lacustrine mudstone	Anhydrite and bassanite [21]
Cumberland (CB)	Lacustrine mudstone	Anhydrite and bassanite [21]
Windjana (WJ)	Reworked fluvial sandstone	Anhydrite and bassanite [22]
Confidence Hills (CH)	Lacustrine mudstone	Jarosite [23]
Mojave (MJ)	Lacustrine mudstone	Jarosite [23]
Telegraph Peak (TP)	Lacustrine mudstone	Jarosite [23]
Buckskin (BK)	Lacustrine mudstone	Anhydrite [23]
Oudam (OU)	Lacustrine sand/siltstone	Anhydrite and gypsum [19]
Big Sky (BS)	Eolian sandstone	Anhydrite [24]
Greenhorn (GH)	Eolian sandstone	Anhydrite and bassanite [24]
Marimba (MB)	Lacustrine mudstone	Anhydrite, bassanite, gypsum, and jarosite [19]
Quela (QL)	Lacustrine mudstone	Anhydrite, bassanite, gypsum, and jarosite [19]
Duluth (DU)	Lacustrine mudstone	Anhydrite and bassanite [17]
Stoer (ST)	Lacustrine mudstone	Anhydrite, bassanite, gypsum, and jarosite [17]
Highfield (HF)	Lacustrine mudstone	Anhydrite, bassanite, and gypsum [17]
Rock Hall (RH)	Lacustrine mudstone	Anhydrite and jarosite [17]
Kilmarie (KM)	Lacustrine mudstone	Anhydrite and bassanite [25]
Glen Etive (GE)	Lacustrine mudstone	Anhydrite and bassanite [25]
Hutton (HU)	Strong diagenetic overprint, grain size indeterminate, and lacustrine	Anhydrite [25]
Edinburg (EB)	Eolian sandstone	None [25]
Glasgow (GG)	Lacustrine mudstone	Anhydrite and bassanite [25]
Mary Anning (MA)	Lacustrine mudstone	Anhydrite and bassanite [25]
Groken (GR)	Lacustrine mudstone	Anhydrite and bassanite [25]

1.1.3. Detection of NaCl and Mg Sulfate in Gale Crater Samples

NaCl has been directly or indirectly detected by MSL instrumentation, including Chemistry and Camera (ChemCam) Laser-Induced Breakdown Spectroscopy (LIBS), the Alpha Particle X-ray Spectrometer (APXS), and CheMin. ChemCam LIBS detected high levels of Cl (above 15 wt.%) in surface targets in the Murray Formation that was positively correlated with Na_2O, suggesting the presence of NaCl [8]. The APXS detected Cl in all the bedrock and eolian targets (typically 0.7 ± 0.4 wt.%) and in diagenetic features (up to ~3 wt.%), e.g., [26,27], although it did not show a systematic geochemical association between Cl and any other single detectable element in the Gale crater bedrock. This suggested that chlorides and/or oxychlorines could be associated with more than one cation [26]. However, a weak positive correlation (r = 0.43) between Cl and Na in targets between theHartmann's Valley and Jura member of the Murray Formation (Figure 1), suggested the presence of NaCl in some samples, although Na oxychlorines could not be ruled out [26]. CheMin detected halite at an abundance of 0.8 wt.% in the Quela drill sample [19]. This was the only detection of a crystalline chloride salt by CheMin as of Sol 2910, meaning that if chlorides were present in other samples, they were below the detection limit of CheMin (~1–2 wt.%) or were X-ray amorphous.

Data collected in-situ by the rover are consistent with the presence of Mg sulfates in some previously analyzed Gale crater rocks, and the orbital data suggest that the rover will traverse over Mg sulfate-rich rocks further in its drive path. ChemCam detected an interval

with elevated and positively correlated abundances of MgO, SO_3, and H (interpreted as hydrated Mg sulfate) in the Murray Formation (between QL and DU) [28], but this interval was not analyzed by SAM because an alternate method of drilling was being developed by engineers in response to an anomaly with the drill [29]. CheMin detected crystalline Fe and Ca sulfates (jarosite, anhydrite, bassanite, and gypsum; Table 1) in multiple samples [16,18,19,21,22,25], but it had not detected crystalline Mg sulfate as of Sol 2910. Finally, polyhydrated and monohydrated Mg sulfates have been detected in the lower section of the LSu in Gale crater (starting at ~25 m above EB; Figure 1) using the Compact Reconnaissance Imaging Spectrometer for Mars (CRISM) on the Mars Reconnaissance Orbiter (MRO) [1,3,4].

1.1.4. HCl and SO_2 Detected by SAM-EGA

HCl

The SAM-EGA instrument detected evolved HCl gas from 25 scooped and drilled Gale crater samples as of Sol 2910, which could be sourced from oxychlorines or chlorides (October 2020) [13,30–34]. Many samples in the Bradbury, Siccar Point, and Mt. Sharp groups evolved O_2 indicative of perchlorate or chlorate thermal decomposition (JK-BK, BS, GH, RH, and EB; Figure 1) [13]. Monocationic oxychlorines thermally decompose into chlorides at temperatures less than 600 °C (e.g., $NaClO_4$; Reaction (1)), after which the chlorides are available to react with other phases.

$$NaClO_4 \rightarrow NaCl + 2O_2 \quad (1)$$

Stratigraphically higher samples further in *Curiosity*'s traverse evolved HCl but no O_2 (OU, MB-KM, HF, and GE-HU; Figure 1), suggesting that oxychlorines were not present in those samples, although chlorides were possible [33,35].

HCl releases above 600 °C in Gale crater samples could be caused by chlorides originally present in the sample or derived from oxychlorine thermal decomposition (Reaction 1), which melted and reacted with water vapor in the oven (Reaction (2)) [36].

$$H_2O_{(g)} + 2NaCl_{(s,l)} \rightleftharpoons 2HCl_{(g)} + Na_2O_{(s)} \quad (2)$$

Laboratory studies have shown that certain oxychlorines and chlorides do not evolve HCl within the SAM temperature range (e.g., $NaClO_4$ and NaCl) when analyzed individually, but they do evolve HCl when mixed with phases that evolve water when heated (e.g., phyllosilicates) [10]. H_2O abundances in Gale crater samples analyzed by SAM-EGA ranged from 0.1 wt.% (Ogunquit Beach) [37] to 3.07 wt.% (Groken) [10,33]) and can be derived from phases such as hydrated salts, phyllosilicates, adsorbed water, and iron oxyhydroxides. These phases produce water peaks at characteristic temperatures during SAM-EGA and are not expected to dehydroxylate prior to SAM analyses (e.g., during drilling), although slightly higher temperatures and lower relative humidity inside CHIMRA could result in some low-temperature water loss [38].

Several Gale crater samples analyzed using SAM-EGA evolved HCl with peaks above 600 °C that sometimes co-evolved with SO_2, suggesting that SO_2-evolving phases, such as sulfates, may affect HCl production in addition to water-evolving phases (Figure 2). The melting point of salts (e.g., nitrates, carbonates) has been shown to decrease when present in multi-phase mixtures [39,40]. Melting chlorides, catalyzed to a lower melting temperature by other phases present in the sample, could then react with water vapor and produce HCl [41]. Additionally, SO_2-evolving phases (e.g., sulfates) are known to react with chlorides and increase HCl production when heated in industrial incinerators [42]. In this reaction, also referred to as "Hargreaves reaction", water vapor (e.g., from kieserite dehydration; Reaction (3)) reacts with the solid or melting chloride (e.g., NaCl) to produce HCl and Na_2O (Reaction (2)) [43]. SO_2 and O_2 sourced from sulfate thermal decomposition (e.g., Mg sulfate; Reaction (4) [44]) can react with the Na_2O, producing sodium sulfate

(Reaction (5)). The consumption of Na_2O shifts Reaction (2) to the right, thereby increasing HCl production.

$$MgSO_4 \cdot H_2O_{(s)} \rightarrow MgSO_{4(s)} + H_2O_{(g)} \quad (3)$$

$$MgSO_{4(s)} \rightarrow MgO_{(s)} + SO_{3(g)} \rightarrow SO_{2(g)} + MgO_{(s)} + 1/2O_{2(g)} \quad (4)$$

$$SO_2 + 1/2O_2 + Na_2O \rightleftharpoons Na_2SO_{4(s,l)} \quad (5)$$

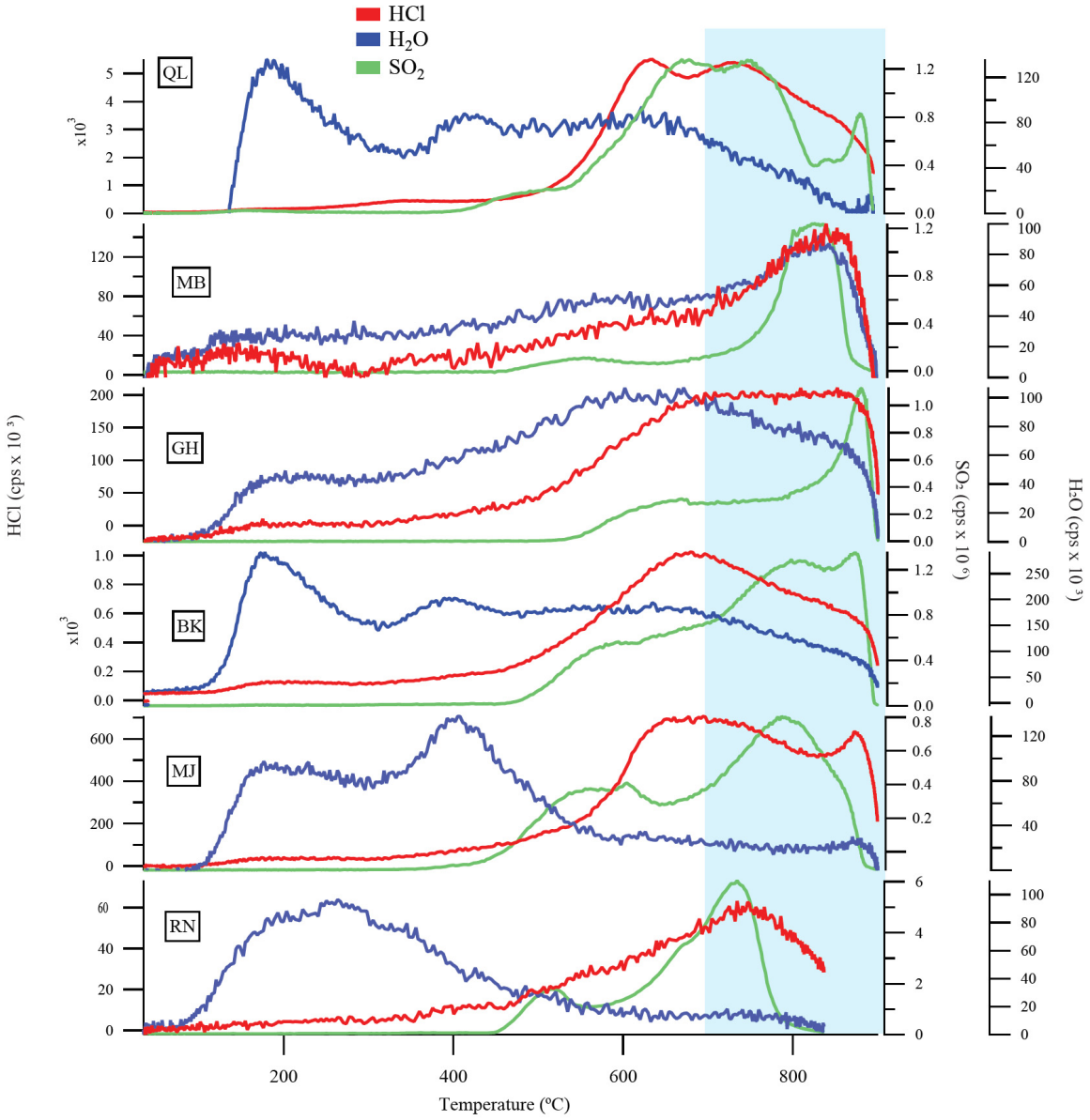


Figure 2. HCl (m/z 36), SO_2 (m/z 64 in RN and MB; m/z 66 in MJ, BK, GH, and QL), and H_2O (m/z 20) evolutions in Gale crater samples analyzed using SAM-EGA. The samples displayed include Rocknest (RN), Mojave (MJ), Buckskin (BK), Greenhorn (GH), Marimba (MB), and Quela (QL). The samples displayed co-evolved SO_2 and HCl above 700 °C (highlighted by the blue box). m/z 66 is an isotopologue of SO_2 and is displayed for MJ, BK, and GH due to the detector being saturated at m/z 64. m/z 20 is an isotopologue of H_2O and is displayed for all samples due to detector saturation at m/z 18. QMS data are shown in counts per second (cps) because masses delivered to the SAM instrument were variable and had a large associated error [13,33,35].

One goal of this work was to investigate whether $MgSO_4$ influenced HCl production from NaCl by (1) lowering its melting temperature and (2) the Hargreaves reaction, and if these HCl releases were produced within the analytical temperature range of SAM.

SO_2

The SAM instrument detected SO_2 releases with peaks above 700 °C in several samples in the Yellowknife Bay, Kimberley, Murray, Stimson, and Carolyn Shoemaker formations (Figure 2). These were not caused by Fe sulfates because laboratory studies demonstrated that Fe sulfates (e.g., jarosite) thermally decompose and release SO_2 at temperatures below 700 °C [45]. Ca sulfate starts thermally decomposing at approximately 1140 °C and rapidly decomposes above 1250 °C [46], which is above the analytical temperature range of the SAM instrument. Mg sulfate analyzed individually thermally decomposes (Reaction (4)) between 880 °C and 1070 °C under a N_2 atmosphere [44], which is also above the temperature range of the SAM instrument. However, previous laboratory studies have demonstrated that other phases (e.g., Fe and Al oxides and perchlorates) catalyze sulfate thermal decomposition to a lower temperature [11,46]. A second goal of this work was to determine whether NaCl catalyzed the thermal decomposition of $MgSO_4$, such that SO_2 was produced within the analytical temperature range of the SAM instrument.

2. Materials and Methods

2.1. Materials and Sample Preparation

Reagent-grade NaCl, confirmed with XRD (Figure S1), was used as an analog to potential chlorides present in Gale crater. Na perchlorate and chlorate thermally decompose into NaCl during sample heating (e.g., Reaction (1)), after which it can react with other phases in the sample. Most Gale crater samples that were interpreted as containing oxychlorines evolved O_2 at a lower temperature than HCl [13]. This suggests that chlorides, and not oxychlorines, were present in the sample at the temperature of HCl production. Therefore, NaCl is also analogous to chlorides derived from monocationic oxychlorines in terms of evolved HCl. NaCl was powdered with a mortar and pestle to below 150 μm, which was the size fraction analyzed by SAM for the samples obtained before the rover transitioned to the use of the feed-extended sample transfer (FEST) sample delivery approach [31], which does not involve sieving samples but still delivers fine powders to the SAM instrument.

Kieserite, a monohydrated Mg sulfate, was chosen as an analog to sulfates present in Gale crater. ESTA kieserite (a natural kieserite extracted from natural salt deposits by the K+S group [47]) was ground into a powder with a particle size of below 150 μm. XRD results showed that this kieserite contained minor NaCl contamination (Figure S2).

Two mixtures of NaCl and kieserite were prepared for the EGA and XRD analyses. The first mixture, called the "equal molar mixture", was made where the number of moles of NaCl and kieserite would theoretically react to completion during sample heating (Reactions (2)–(5)) without excess reactants (moles NaCl/moles kieserite = 2). The second mixture, called the "Mars-like mixture", had a NaCl-to-kieserite ratio that roughly approximated the ratio of chlorides to Mg sulfates in select Gale crater samples (moles NaCl/moles kieserite $\approx$ 0.5). The primary purpose of this mixture was to determine the effect of excess sulfate reactant on EGA and XRD results, and therefore a lower NaCl/kieserite molar ratio was used. This ratio was calculated by assuming all Cl detected by the APXS in drill dump piles was in NaCl. Approximate Mg sulfate abundances were determined by subtracting Ca sulfate contributions (from CheMin data) from total APXS SO_3, and then subtracting SAM SO_3 that was not attributed to Mg sulfate (i.e., SO_2 releases < 700 °C). Both mixtures were prepared by powdering NaCl and kieserite and then mechanically mixing them with a mortar and pestle.

2.2. Laboratory Thermal and Evolved Gas Analysis

NaCl, kieserite, and the two NaCl/kieserite mixtures were analyzed for their evolved gases for the purpose of comparing them with the SAM-EGA data. The dry, powdered

samples (~19–20 mg) were placed in 150 µL alumina crucibles. The sample crucible and an identical empty reference crucible were heated in a Setaram Labsys EVO differential scanning calorimeter (DSC)/thermal gravimeter (TG) connected to a Pfeiffer ThermoStar quadrupole mass spectrometer (QMS) for the evolved gas analysis. The Labsys DSC was calibrated for the furnace temperature and endo/exotherm peak areas using a set of five metal calibration standards. SAM does not have a TG/DSC, but these additional instrument capabilities were used to better understand the phase transitions and reactions in the laboratory samples. The instrument operating parameters, including furnace pressure, carrier gas, and heating rate, were set to be similar to the SAM instrument on the *Curiosity* rover to ground-truth SAM-EGA data with high fidelity. Low furnace pressures were achieved by using a low carrier gas flow rate (He, 10 sccm) and vacuum pumps. The furnace pressure was set to 30 mbar, and the samples were heated from ~30 °C to 1000 °C at a heating rate of 35 °C/min. All samples were run in duplicate.

2.3. Laboratory-Powered X-ray Diffraction Analysis

Powdered samples were analyzed with the PANalytical X'Pert Pro MPD XRD for mineral phase identification with an X'celerator detector and a Co Kα radiation tube. Data were collected from 4 to 80 degrees 2θ at 40 mA and 45 kV at a step size of 0.02°. The XRD instrument was operated under ambient conditions on a spinner stage. The same XRD analytical parameters were used for the non-ambient analyses described next.

These samples were also analyzed on the PANalytical instrument using the Anton Paar XRK 900 heating stage to observe the mineralogical phase changes caused by sample heating. The samples were analyzed in N_2-purged cells (~10 sccm; high purity K-bottle source) starting at a temperature of 25 °C and then heated to 250 °C. The cell temperature was held at 250 °C for 5 min, and then the sample was reanalyzed. The cell temperature was programmed to heat samples to 900 °C at a rate of 60 °C/min using 25 °C intervals. The samples were held at each temperature step for 5 min, analyzed (2.08 min per analysis), and then ramped to the next temperature. These samples, referred to as the "post-heat" samples, were then cooled to 25 °C in the cell without exposure to lab air and reanalyzed. The heating profile was stepwise rather than constant (like the EGA) because temperatures must be held constant during each XRD measurement. Mineral identification was accomplished using HighScore v. 4.7 software by comparing the XRD patterns to the patterns from the International Centre for Diffraction Data (ICDD) database and the Crystallography Open Database (COD). The XRD patterns at each heating step were compared to each other to observe how the sample mineralogy changed during heating.

The XRD analyses of the heated samples were intended to aid in the interpretation of the laboratory-evolved gas analysis results. The XRD analyses of the heated samples showed which phases formed, decomposed, or melted during heating and the order in which they were present. This information was used to understand the phase changes and chemical reactions reflected in the DSC and evolved gas data. It is important to note that the different instrumental conditions between the XRD of heated samples and EGA (e.g., heating rate) may have led to discrepancies between the temperatures at which phase changes and reactions occurred. Primarily, the stepwise heating program in the XRD experiments may allow more time for the sample to decompose and for reactions to occur at each temperature step; therefore, these changes may be observed at lower temperatures than they would in the EGA experiments. Additionally, XRD has a higher detection limit than EGA, and data quality may be affected by factors that affect the sample height (e.g., melting of phases, expansion during heating, and volatilization of phases). Although temperature discrepancies are expected between these two methods, the XRD of heated samples is useful for identifying the types of phases present and the order in which they appear during heating, which ultimately aids in the interpretation of the laboratory thermal and evolved gas data.

3. Results

3.1. NaCl

NaCl analyzed individually did not evolve HCl, SO_2, or H_2O within the tested temperature range, and produced a melting endotherm peak at 823 °C and a volatilization endotherm peak at 961 °C, both consistent with literature values (Figure 3) e.g., [48]. The melting endotherm was larger in NaCl analyzed individually than in the mixtures because the amount of NaCl in the sample crucible was greater. A total of ~19–20 mg NaCl was analyzed in the crucible during the thermal and evolved gas analysis, which equated to 0.34 µmol NaCl as opposed to 0.16 µmol NaCl in the equal molar mixture and 0.06 µmol NaCl in the Mars-like mixture. The XRD results of the heated NaCl demonstrated that that NaCl was not detected above 800 °C (Figures 4 and S1), which was consistent with the melting of NaCl. No peaks were detected in the XRD data from the post-heat NaCl sample measured at 25 °C, which was consistent with its complete volatilization.

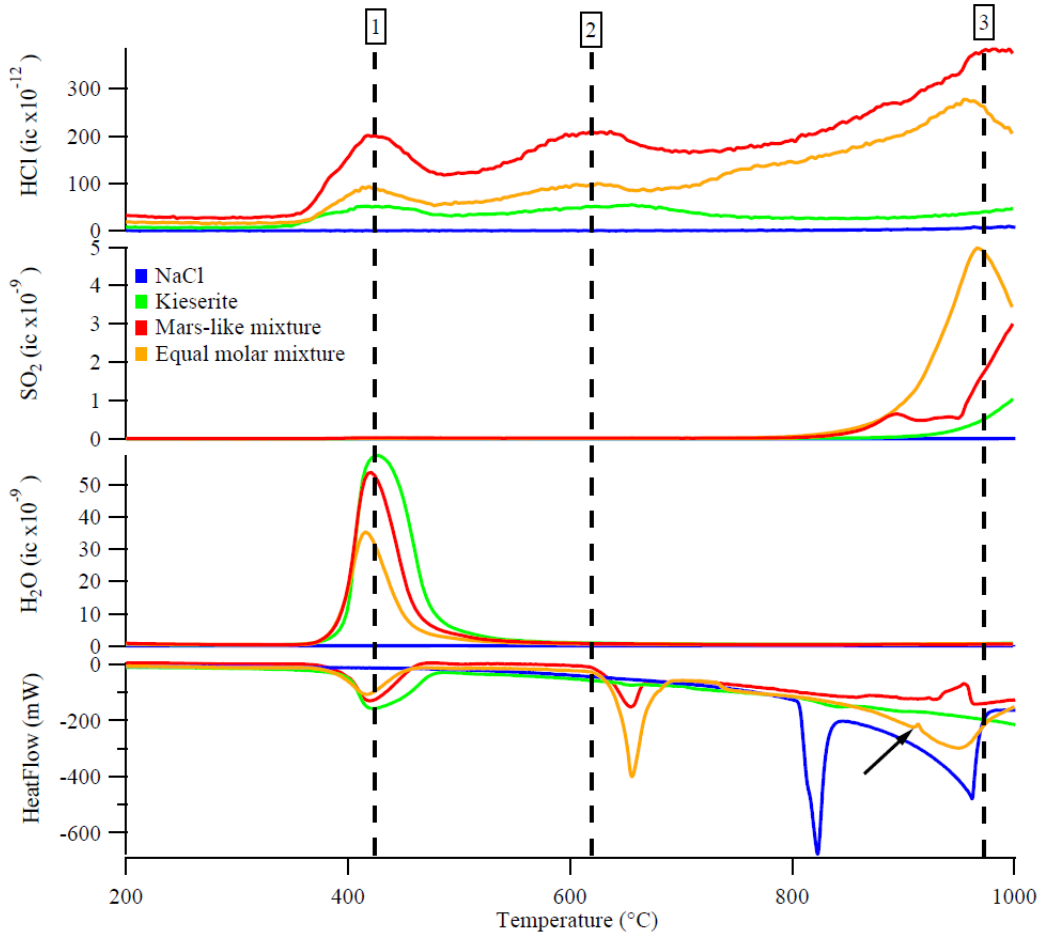


Figure 3. Laboratory-evolved HCl, SO_2, H_2O, and DSC heat flow data from NaCl, kieserite, the equal molar NaCl/kieserite mixture, and the Mars-like NaCl/kieserite mixture. ic = ion current (amperes). The HCl peaks are labeled 1, 2, and 3 for ease of viewing. The arrow points to a small exotherm in the equal molar mixture DSC data.

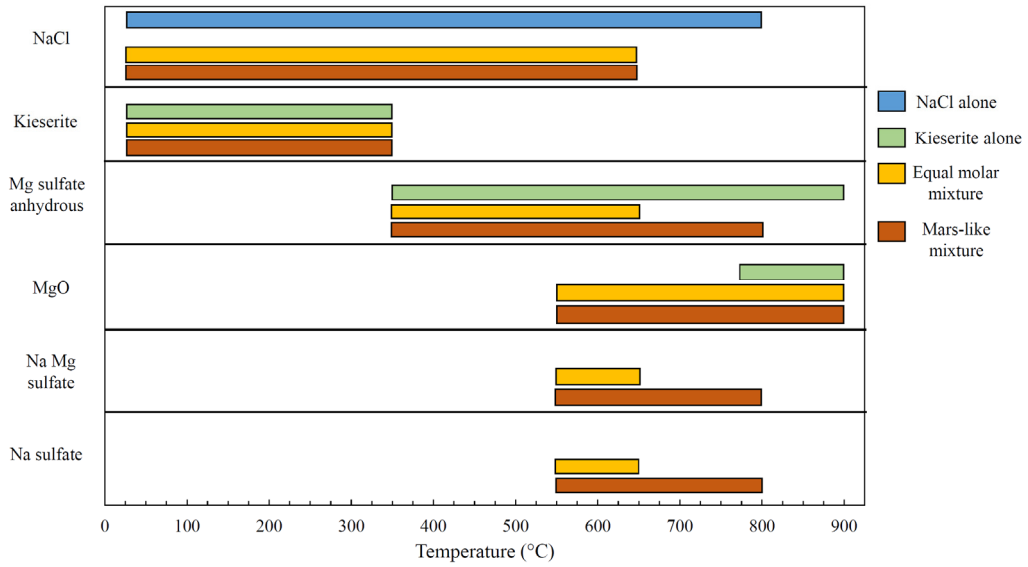


Figure 4. The XRD results of heated samples show crystalline phases present at temperatures ranging from 25 °C to 900 °C, with a 25 °C step size above 250 °C. The results are shown for NaCl, kieserite, the equal molar NaCl/kieserite mixture, and the Mars-like NaCl/kieserite mixture.

3.2. Kieserite

The thermal and evolved gas analysis and XRD results demonstrated that kieserite dehydrated at ~350 °C and then incompletely decomposed into MgO (periclase) at higher temperatures (Figure S2) Kieserite analyzed individually evolved a relatively small amount of HCl, but this was due to the minor NaCl contamination that was detected by XRD in this natural sample (Figure S2). Kieserite evolved water from dehydration that started at a temperature of ~350 °C and peaked at 423 °C (Figure 3). Kieserite analyzed individually produced a dehydration water release with a greater area than in the two mixtures due to the greater amount of kieserite used in the sample crucible. A total of ~19–20 mg kieserite was analyzed in the crucible during the thermal and evolved gas analysis, which equated to 0.14 µmols kieserite as opposed to 0.11 µmols kieserite in the Mars-like mixture and 0.08 µmols kieserite in the equal molar mixture (Figure 3). The EGA results were consistent with kieserite no longer being detected by XRD above 350 °C (Figure 4). Anhydrous Mg sulfate ($MgSO_4$) was detected by XRD from 350 °C to 875 °C and possibly 900 °C (Figure 4).

XRD detected periclase (MgO) from 800 °C (possibly 775 °C) to 900 °C due to the decomposition of anhydrous Mg sulfate (Reaction 4). Anhydrous Mg sulfate and periclase peaks were also detected by XRD in the post-heat sample measured at 25 °C. The overlap between the detection of anhydrous Mg sulfate and MgO may be attributed to the gradual decomposition of anhydrous Mg sulfate into MgO.

The SO_2 release that started at a temperature of ~900 °C and peaked above 1000 °C was attributed to anhydrous Mg sulfate decomposing into MgO (Figure 3; Reaction (4)). The slight discrepancy between the temperature at which MgO was detected by XRD and the temperature at which SO_2 was detected by EGA was likely due to the different pressures and heating rates between these two analyses. It should also be noted that only minor MgO peaks were detected using XRD at temperatures below 875 °C (Figure S2), indicating that the majority of anhydrous Mg sulfate decomposition occurred at or above 875 °C. Despite slight temperature discrepancies, the XRD results demonstrated that the likely source of evolved SO_2 was the thermal decomposition of $MgSO_4$ into periclase, O_2, and SO_2 (Reaction (4)).

3.3. Equal Molar Mixture

The equal molar mixture of NaCl and kieserite (moles NaCl/moles kieserite = 2) evolved HCl with three peaks as well as SO_2, described below. The XRD results of the heated

samples are shown in Figure S3. The sample crucibles for the thermal and evolved gas analysis contained ~19–20 mg of the mixture, which equated to approximately 0.16 µmols NaCl and 0.08 µmols kieserite.

HCl peak 1: The first HCl release peak (419 °C) from the equal molar mixture of NaCl and kieserite was caused by the reaction between kieserite dehydration water and solid NaCl (Reaction (2); Figure 3). The XRD patterns of the heated equal molar mixture showed that kieserite was detected until 350 °C and anhydrous Mg sulfate formed at 350 °C (Figure 4). The calorimetry and evolved gas analysis results from the equal molar mixture showed a water release peak and an endotherm at 415 °C, also indicative of kieserite dehydration. Previous studies demonstrated that Reaction (2) can occur and increase HCl production even below the melting point of chlorides.

HCl peak 2: The second HCl peak (624 °C) in the equal molar mixture was likely caused by the increased reactivity of NaCl with water vapor due to the melting of NaCl. The second HCl release peak co-occurred with an endotherm (peak at 654 °C), indicative of NaCl melting (Figure 3). Additionally, NaCl was not detected by XRD above 650 °C, which is consistent with melting (Figure 4). NaCl analyzed individually melts at ~800 °C; however, multi-phase mixtures are known to decrease individual salt melting temperatures [39,40]. The melting endotherm in the equal molar mixture was larger than the Mars-like mixture due to the greater amount of NaCl in the sample crucible during EGA (0.16 µmol as opposed to 0.06 µmol, respectively).

HCl peak 3: The third HCl release peak (957 °C) in the equal molar mixture was caused by the reaction between Na_2O, MgO, and SO_2 (the products of Reactions (2) and (4)), which drove the production of Na sulfate (Na_2SO_4), Na–Mg sulfate ($Na_2Mg(SO_4)_2$), and HCl (i.e., Hargreaves reaction; Reactions (2), (5) and (6)). Na sulfate has also been shown to be a product of gaseous NaCl and SO_2 [49]. The large endotherm (peak at 948 °C) was caused by a combination of Mg sulfate, Na sulfate, and Na–Mg sulfate thermal decomposition and NaCl volatilization.

$$2SO_2 + O_2 + Na_2O + MgO \rightarrow Na_2Mg(SO_4)_2 \quad (6)$$

SO_2 peak 1: The equal molar mixture evolved SO_2 with a peak at 970 °C, which was a lower temperature than kieserite analyzed individually (Figure 3). This suggested that NaCl catalyzed the thermal decomposition of Mg sulfate o a lower temperature. The XRD results of the heated equal molar mixture showed that anhydrous Mg sulfate was detected from 350 °C to 650 °C, and Na sulfate and Na–Mg sulfate were detected from 575 °C (possibly 550 °C) to 650 °C. Na sulfate and Na–Mg sulfate were formed by the reaction between SO_2 from Mg sulfate thermal decomposition, Na_2O, and MgO (Reactions (5) and (6)). Any Na sulfate that was formed through the Hargreaves reaction would melt at or below ~880 °C (thus no longer being detected by XRD) and then evolve SO_2 (Figure 5) [50]. Therefore, the SO_2 release observed in the EGA results from the equal molar mixture was likely the product of the thermal decomposition of multiple sulfate phases (Mg sulfate, Na sulfate, and Na–Mg sulfate). Additionally, there was a small DSC exotherm within the larger endotherm from sulfate decomposition (arrow in Figure 3) that may be caused by changes in Mg sulfate crystal structure [44,51].

MgO, the product of anhydrous Mg sulfate decomposition, was detected by XRD from 550 °C to the maximum analytical temperature of 900 °C, suggesting gradual Mg sulfate decomposition. However, it should be noted that the MgO peaks in the XRD data were minor until ~675 °C (Figure S3). The post-heat equal molar mixture analyzed with XRD at 25 °C only contained MgO, suggesting complete thermal decomposition of the sulfate.

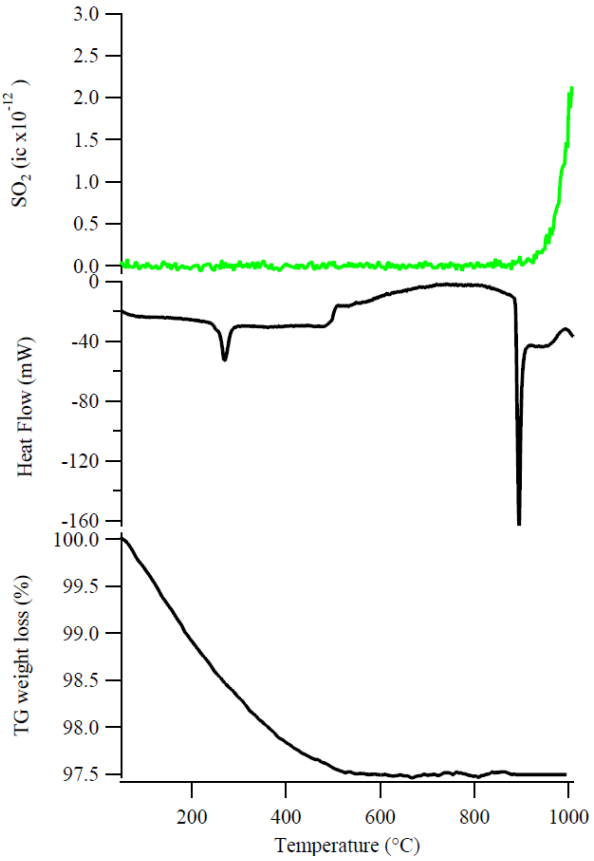


Figure 5. Evolved SO_2, TG, and DSC data from sodium sulfate hydrate analyzed using a TG/DSC/mass spectrometer instrument configured to operate under similar conditions as the SAM instrument. ic = ion current (amperes).

3.4. Mars-like Mixture

The Mars-like mixture of NaCl and kieserite (moles NaCl/moles kieserite ≈ 0.5) also evolved a HCl release with three distinct peaks (Figure 3) and SO_2, which are described below. The XRD results of the heated samples are shown in Figure S4. The sample crucibles used in the thermal and evolved gas analysis contained ~19–20 mg of this mixture, which equated to approximately 0.06 µmols NaCl and 0.11 µmols kieserite. The HCl evolutions were fairly similar to the equal molar mixture, even with the excess sulfate.

HCl peak 1: The first HCl release peak (424 °C) in the Mars-like mixture of NaCl and kieserite was attributed to the reaction between kieserite dehydration water and the solid NaCl, similar to the first HCl release observed in the equal molar mixture of NaCl and kieserite. This is supported by the co-evolution of H_2O (peak at 421 °C) and HCl in the EGA data (Figure 3), in addition to the transition from kieserite to anhydrous Mg sulfate at 350 °C in the XRD data (Figure 4). The first HCl release from the Mars-like mixture was slightly larger in magnitude compared to the equal molar mixture due to the higher kieserite-to-NaCl ratio, leading to increased H_2O that could come into contact and react with solid NaCl.

HCl peak 2: The second HCl release peak (627 °C) in the Mars-like mixture of NaCl and kieserite was attributed to melted NaCl reacting with water vapor, similar to the equal molar mixture. This was supported by an endotherm (peak at 654 °C) observed in the DSC data and the disappearance of NaCl above 650 °C in the XRD data. The 654 °C endotherm was smaller in the Mars-like mixture compared to the equal molar mixture because there was less NaCl (0.06 µmol in the Mars-like mixture as opposed to 0.16 µmol in the equal molar mixture).

HCl peak 3: The third HCl release peak in the Mars-like mixture, similar to the equal molar mixture, was attributed to SO_2 driving the reaction between NaCl and water (Reactions (4)–(7)). The third HCl release started at ~740 °C and peaked at 983 °C (Figure 3). This coincided with the overall SO_2 release, which had peaks at ~891 °C and above 1000 °C (Figure 3).

SO_2 peak 1: The first SO_2 peak produced from the Mars-like mixture could be caused by the decomposition of anhydrous Mg sulfate. Anhydrous Mg sulfate may have started to decompose at or below ~800 °C, producing SO_2, which reacted with Na_2O and/or MgO to form Na sulfate and Na–Mg sulfate (Reactions (5)–(6)). Both Na–Mg sulfate and Na sulfate were detected by XRD between 575 °C and 800 °C (Figure 4; Reactions (7) and (8)), which was a wider temperature range than the equal molar mixture. This may be caused by the lower relative amount of NaCl available to catalyze sulfate thermal decomposition to a lower temperature. MgO was detected by XRD from 550 °C to 900 °C. The overlap between the detection of anhydrous Mg sulfate and MgO was likely due to the gradual decomposition of the sulfate into MgO.

SO_2 peak 2: The second SO_2 peak may be caused by Na sulfate and Na–Mg sulfate thermal decomposition, in addition to excess Mg sulfate thermal decomposition. The excess of anhydrous Mg sulfate was caused by excess kieserite reactant in the original mixture. The broad downward deflection in the DSC data (starting at ~730 °C) was smaller in the Mars-like mixture than the equal molar mixture because there was less NaCl volatilization, and sulfate decomposition was not complete at 1000 °C. The small exotherm observed within the larger downward deflection may be caused by the formation of Na sulfate and Na–Mg sulfate, which subsequently decomposed. This exotherm may be obscured by the larger endotherm in the equal molar mixture.

4. Discussion

4.1. Comparison with Gale Crater Samples

Overall, the laboratory results from this work demonstrated that $MgSO_4$ and NaCl evolved gases (SO_2 and HCl, respectively) within the SAM-EGA temperature range when mixed, whereas $MgSO_4$ and NaCl analyzed individually did not. Previous work demonstrated that evolved HCl detected by SAM-EGA can be caused by melting chlorides reacting with water vapor from phases such as phyllosilicates. However, the cause of HCl releases in the Gale crater samples that had multiple peaks above 600 °C, such as the examples displayed in Figure 6, was not well understood. This work demonstrated that HCl releases above 600 °C detected by SAM-EGA are complex and may be caused by multiple mechanisms that involve sulfates. All samples analyzed by SAM-EGA in Gale crater evolved high-temperature HCl, and the variation in their release patterns was likely the result of interactions between chlorides and other phases present in the sample, such as Mg sulfates.

One mechanism for HCl production from NaCl is the reaction between water vapor and melting chlorides, catalyzed to a lower temperature by sulfates. Results demonstrated that the melting point of NaCl decreases when Mg sulfate is present, making it more reactive with water vapor. Broad HCl releases with peaks ranging from 500 to 700 °C occurred in most samples analyzed by SAM. Greenhorn (GH) and Quela (QL) are examples of samples analyzed by SAM-EGA in Gale crater that evolved HCl with peaks between approximately 600 and 700 °C and were similar to those observed in the laboratory mixtures (Figure 6). The HCl peaks labeled "1" may be caused by melting chlorides, catalyzed to a lower melting point by sulfates, reacting with water vapor (Figure 6). Chlorides in these types of samples may be originally present in the sample, like in QL [13], or derived from oxychlorine thermal decomposition, like in GH [13], depending on whether there was also evolved O_2 below 600 °C.

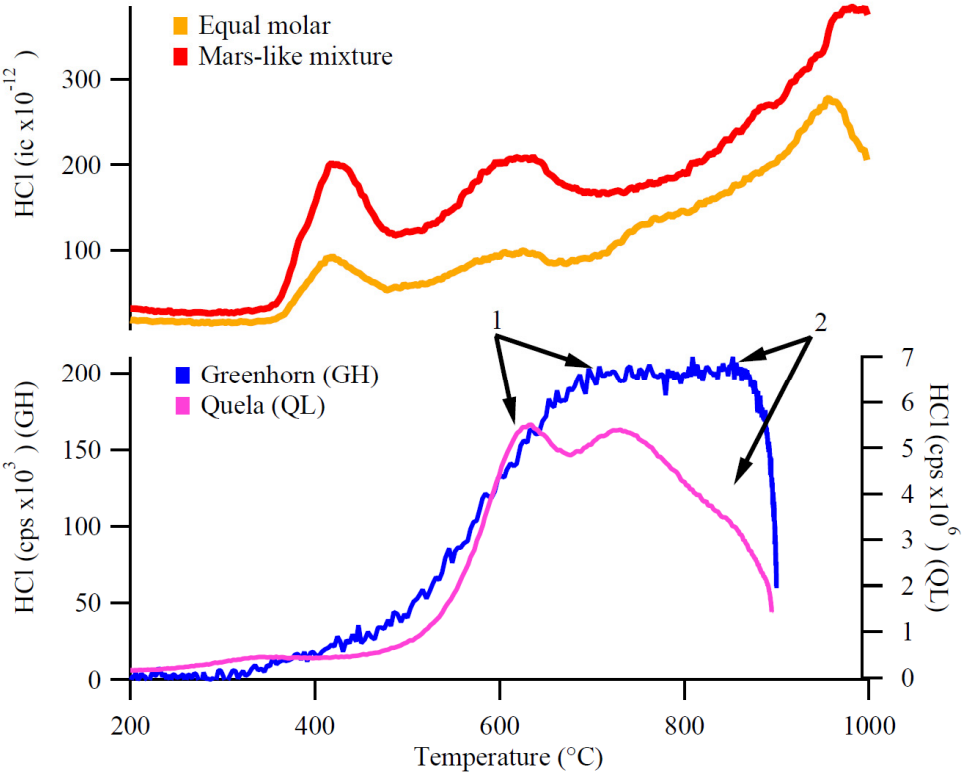


Figure 6. HCl evolutions from laboratory "equal molar" and "Mars-like" mixtures compared to HCl releases from Gale crater samples (Greenhorn and Quela) analyzed using SAM-EGA. Greenhorn and Quela are examples of Gale crater samples that evolved high-temperature HCl similar to the laboratory samples. HCl peaks labeled "1" may be caused by melting chlorides reacting with water vapor in the SAM oven, and "2" points to apparent HCl peaks that may be caused by chlorides reacting with SO_2 from partial Mg sulfate decomposition. The SAM QMS data are shown in counts per second (cps) because masses delivered to the SAM instrument were variable and had a large associated error [13,33,35].

A second mechanism of HCl production in SAM-EGA is the reaction between $SO_{2(g)}$ (from sulfate decomposition), chlorides, and water vapor (i.e., "Hargreaves reaction"). Figure 6 shows two examples of Gale crater samples that also evolved HCl above 800 °C, similar to those observed in the laboratory mixtures. The sharp decrease in HCl counts at the maximum temperature is due to the sudden cessation of heating in the SAM oven, resulting in apparent peaks. These apparent HCl peaks may only represent the beginning of a larger HCl release that would peak at a higher temperature if heating continued and would more closely resemble the evolved HCl from the laboratory mixtures. HCl above 800 °C in these Gale crater samples may have been caused by a Hargreaves-type reaction.

These results also demonstrated the catalytic effect of NaCl on $MgSO_4$ thermal decomposition, which is essential for its detection in Gale crater samples using SAM-EGA. SO_2 releases in the two laboratory mixtures started at approximately 800 °C and peaked above the maximum temperature analyzed by SAM-EGA (~870 °C). Scooped samples including Rocknest (RN) and drilled samples including Confidence Hills (CH), Mojave (MJ), Buckskin (BK), Greenhorn (GH), Marimba (MB), and Quela (QL) evolved high-temperature SO_2 (>700 °C), similar to those observed in the laboratory mixtures of NaCl and Mg sulfate (Figures 2 and 7). In SAM-EGA data, partial Mg sulfate thermal decomposition would appear as sharp, high-temperature SO_2 releases, similar to the peaks labeled "1" in Figure 7, due to the sudden drop in oven temperature once heating ceases. These apparent SO_2 peaks may only represent the beginning of a larger SO_2 release that would peak at a higher temperature if heating continued and would more closely resemble the evolved SO_2 from the laboratory mixtures.

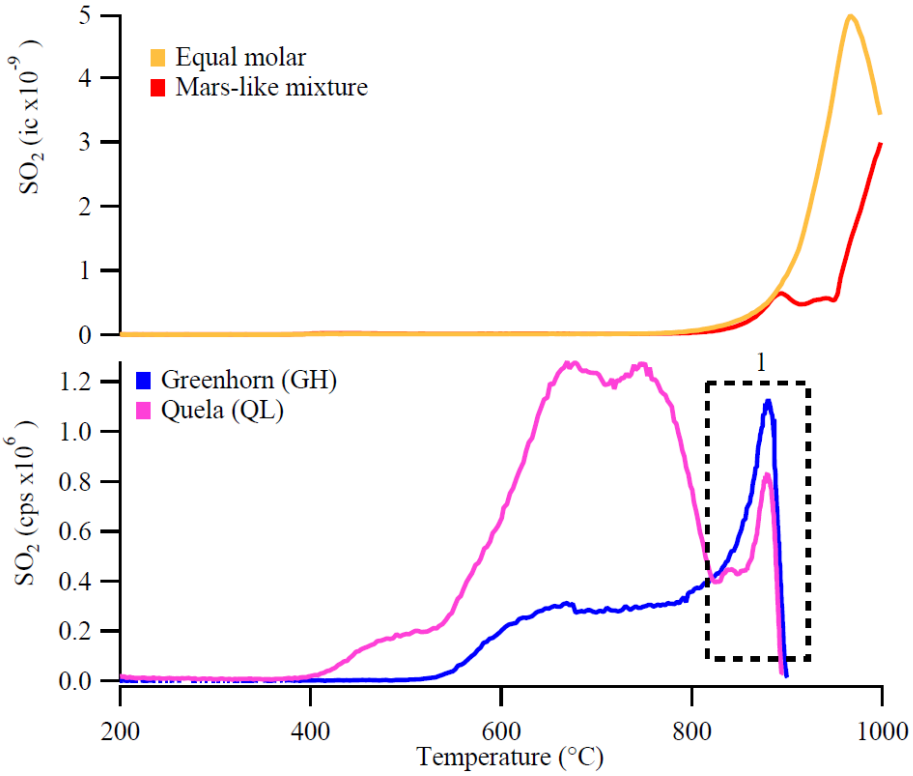


Figure 7. SO_2 evolutions from laboratory "equal molar" and "Mars-like" mixtures compared to SO_2 releases from Gale crater samples (Greenhorn and Quela) analyzed using SAM-EGA. Greenhorn and Quela are examples of Gale crater samples that evolved high-temperature SO_2, similar to the laboratory samples. Apparent SO_2 peaks in the rectangle labeled "1" may be caused by the start of Mg sulfate thermal decomposition catalyzed to a lower temperature by chlorides. Partial Mg sulfate decomposition may result in apparent peaks due to the cessation of oven heating. SO_2 peaks below 700 °C may be caused by sulfates that decompose at lower temperatures (e.g., Fe sulfates). The SAM QMS data are shown in counts per second (cps) because masses delivered to the SAM instrument were variable and had a large associated error [13,33,35].

4.2. Implication of Detecting Mg Sulfates and Chlorides in Gale Crater

The detection of NaCl and Mg sulfate by SAM-EGA is important when Mg sulfates and chlorides are undetectable by other rover instruments because these minerals can provide information about past climate and secondary mineral formation conditions. Hydrated Mg sulfates are sensitive to changes in relative humidity, pressure, pH, and temperature and are thus good indicators of past mineral formation conditions. This work demonstrated that $MgSO_4$ is detectable by SAM-EGA when mixed with chlorides, and the hydration state can potentially be determined from low-temperature water peak integrations. For example, epsomite ($MgSO_4 \cdot 7H_2O$) and hexahydrite ($MgSO_4 \cdot 6H_2O$), both common and stable on the Earth's surface, transition both directions based on relative humidity and temperature (e.g., epsomite transitions to hexahydrite at 50%–55% relative humidity at 298 K [52]). With increasing relative humidity, kieserite transforms into hexahydrite or epsomite, but this transformation is not easily reversible [6].

Kieserite is an especially good environmental indicator because it is stable at lower relative humidity and at higher temperatures [6]; the evolved gas analysis in this work demonstrated that it is stable to a temperature of ~350 °C at 30 mbar. Kieserite can form from hexahydrite or starkeyite ($MgSO_4 \cdot 4H_2O$) in arid environments exposed to heat (e.g., sunlight, geothermal heating) [7]. Kieserite mixed with NaCl evolved SO_2 starting at a temperature of ~800 °C and a distinct water release at a temperature of about 350 °C (Figure 3), thus making it detectable by SAM-EGA.

Chlorides and Mg sulfates also provide important information about the past climate and secondary mineral formation conditions, especially when sedimentary and/or textural features in the rocks are observed (e.g., the abundance of veins, nodules, and laminations). If chlorides and sulfates are detected in specific strata with evidence of desiccation (e.g., desiccation cracks), this would signify a particularly drier period in Mars' history. Morphological features consistent with a transition to arid conditions, including desiccation cracks, have been observed in the Sutton Island member of the Murray Formation, indicating periods of intermittent exposure [53]. Laterally extensive and macroscopic chloride or Mg sulfate deposits have not been observed by *Curiosity*, suggesting that Mg sulfates and NaCl detected in samples previously analyzed by SAM-EGA formed through leaching/reprecipitation or diagenetic processes. These evaporitic layers may exist higher in the LSu, or chloride and Mg sulfate layers may have dissolved and reprecipitated during diagenetic processes [8]. If chlorides and Mg sulfates are detected sporadically rather than across a laterally continuous layer, or in areas with concentrated diagenetic features (e.g., nodules and veins), this could indicate that they precipitated from diagenetic fluids or were derived from soil-formation processes, such as from acid–sulfate weathering of basalts [9].

Finally, the detection of chlorides and sulfates is important because of their implications for past habitability and the possible preservation of organic compounds. Salts such as halite and sulfates commonly preserve signs of past microbial life on Earth e.g., [54,55] and may also preserve biosignatures on Mars. Inclusions in buried salt crystals are an ideal microenvironment for the preservation of microbes due to their protection from radiation and the presence of hypersaline fluids and low oxygen content [55,56]. Viable prokaryotes have been extracted from fluid inclusions inside relatively unaltered terrestrial halite crystals that were millions of years old [55]. Additionally, DNA and RNA fragments have been detected in terrestrial halite crystals up to 435 Ma [57]. However, laboratory experiments have found that ionizing radiation can damage certain bacterial spores on Mars and can limit their survival to 600,000 years in the uppermost meter and up to 160 Ma if located 3 m below the Martian surface [58,59]. Nonetheless, the detection of sulfates and NaCl by SAM-EGA can provide directions on where to drill and analyze for organic compounds with GCMS. This can provide further information about past habitability and is especially relevant when the *Curiosity* rover analyzes rocks within the LSu.

5. Conclusions

Kieserite/NaCl mixtures were analyzed on a laboratory TG/DSC/mass spectrometer instrument configured to operate under similar conditions as SAM to determine if interactions during heating affected evolved HCl and SO_2. The results demonstrated that HCl releases with peaks above 600 °C observed in SAM-EGA data are complex and caused by a combination of phase changes and chemical reactions. The samples analyzed by SAM-EGA in Gale crater that evolved HCl with peaks above 600 °C could be caused by chloride melting due to the catalytic effect of sulfates, making them more reactive with water vapor in the SAM oven. Additionally, SO_2 from Mg sulfate thermal decomposition may react with chlorides and increase HCl production due to a Hargreaves-type reaction. The results from this work suggested that SO_2 from Mg sulfate thermal decomposition can react with Na_2O (the product of NaCl and H_2O) and MgO (from $MgSO_4$ thermal decomposition) and produce Na sulfate, Na–Mg sulfate, and HCl. Furthermore, this work demonstrated that NaCl catalyzes the thermal decomposition of Mg sulfate, such that SO_2 started evolving within the temperature range of SAM (<~870 °C). SO_2 is likely caused by the thermal decomposition of Mg sulfate, Na sulfate, and Na–Mg sulfate produced from reactions during heating. Overall, these results demonstrated that mixtures of NaCl and Mg sulfate evolved gases (HCl and SO_2) within the temperature range analyzed by SAM-EGA, thus making them detectable. Detections of NaCl and Mg sulfate can provide information on past climate and mineral formation conditions (e.g., pH, temperature, and relative humidity).

Supplementary Materials: The following supporting information can be downloaded at: https://www.mdpi.com/article/10.3390/min14030218/s1, Figure S1: XRD results from heated NaCl analyzed individually; Figure S2: XRD results from heated kieserite analyzed individually; Figure S3: XRD results from the heated equal molar mixture; Figure S4: XRD results from the heated Mars-like mixture.

Author Contributions: Conceptualization J.V.C.; methodology, J.V.C. and B.S.; formal analysis, J.V.C. and P.C.; investigation, J.V.C. and B.S.; data curation, J.V.C.; writing—original draft preparation, J.V.C.; writing—review and editing, J.V.C., B.S., A.C.M., C.A.K., V.M.T., P.D.A., E.B.R., D.W.M. and P.C.; visualization, J.V.C.; project administration, P.R.M. and C.M.; funding acquisition, E.B.R. All authors have read and agreed to the published version of the manuscript.

Funding: This research was funded by the Mars Science Laboratory project.

Data Availability Statement: SAM data are publicly available through the NASA Planetary Data System at http://pds-geosciences.wustl.edu/missions/msl/sam.htm (accessed on 25 January 2024), which was updated in March 2022. The data used to make graphs in this manuscript are publicly available on https://dataverse.harvard.edu/dataset.xhtml?persistentId=doi:10.7910/DVN/CNBSYY (accessed on 25 January 2024). This manuscript did not utilize software that had a significant impact on the research.

Acknowledgments: The authors are grateful to the engineers and scientists of the MSL *Curiosity* team, who have made the mission possible and the reported data available.

Conflicts of Interest: The authors declare no conflict of interest. The funders had no role in the design of the study; in the collection, analyses, or interpretation of data; in the writing of the manuscript; or in the decision to publish the results.

References

1. Milliken, R.E.; Grotzinger, J.P.; Thomson, B.J. Paleoclimate of Mars as captured by the stratigraphic record in Gale Crater. *Geophys. Res. Lett.* **2010**, *37*. [CrossRef]
2. Powell, K.E.; Arvidson, R.E.; Edwards, C.S. Spectral Properties of the Layered Sulfate-Bearing Unit in Mount Sharp, Gale Crater, Mars. In Proceedings of the Lunar and Planetary Science Conference, Houston, TX, USA, 13–17 March 2023.
3. Sheppard, R.Y.; Milliken, R.E.; Robertson, K.M. Presence of clay minerals can obscure spectral evidence of Mg sulfates: Implications for orbital observations of Mars. *Icarus* **2022**, *383*, 115083. [CrossRef]
4. Fraeman, A.A.; Ehlmann, B.L.; Arvidson, R.E.; Edwards, C.S.; Grotzinger, J.P.; Milliken, R.E.; Quinn, D.P.; Rice, M.S. The stratigraphy and evolution of lower Mount Sharp from spectral, morphological, and thermophysical orbital data sets. *J. Geophys. Res. Planet.* **2016**, *121*, 1713–1736. [CrossRef] [PubMed]
5. Gupta, S.; Dietrich, W.E.; Lewis, K.W.; Kite, E.; Mondro, C.A.; Schieber, J.; Weitz, C.; Bryk, A.B.; Edgar, L.; Fedo, C.; et al. "High" but not so dry on Aeolis Mons: Transient lake systems in Hesperian deserts in Gale Crater. In Proceedings of the Lunar and Planetary Science Conference, Houston, TX, USA, 13–17 March 2023.
6. Vaniman, D.; Bish, D.; Chipera, S.J.; Fialips, C.I.; Carey, J.W.; Feldman, W.C. Magnesium sulphate salts and the history of water on Mars. *Nature* **2004**, *431*, 663–665. [CrossRef] [PubMed]
7. Chipera, S.J.; Vaniman, D. Experimental stability of magnesium sulfate hydrates that may be present on Mars. *Geochim. Cosmochim. Acta* **2007**, *71*, 241–250. [CrossRef]
8. Thomas, N.H.; Ehlmann, B.L.; Meslin, P.Y.; Rapin, W.; Anderson, D.E.; Rivera-Hernandez, F.; Forni, O.; Schroeder, S.; Cousin, A.; Mangold, N.; et al. Mars Science Laboratory Observations of Chloride Salts in Gale Crater, Mars. *Geophys. Res. Lett.* **2019**, *46*, 10754–10763. [CrossRef] [PubMed]
9. Tosca, N.J.; McLennan, D.; Lindsley, D.H.; Schoonen, M.A. Acid-sulfate weathering of synthetic Martian basalt: The acid fog model revisited. *J. Geophys. Res. Planets* **2004**, *109*. [CrossRef]
10. Clark, J.V.; Sutter, B.; McAdam, A.C.; Rampe, E.B.; Archer, P.D.; Ming, D.W.; Navarro-Gonzalez, R.; Mahaffy, P.; Lapen, T.J. High-Temperature HCl Evolutions From Mixtures of Perchlorates and Chlorides With Water-Bearing Phases: Implications for the SAM Instrument in Gale Crater, Mars. *J. Geophys. Res. Planet.* **2020**, *125*, e2019JE006173. [CrossRef]
11. McAdam, A.; Knudson, C.; Sutter, B.; Franz, H.; Archer, P.D.; Eigenbrode, J.; Ming, D.W.; Morris, R.; Hurowitz, J.A.; Mahaffy, P. Reactions involving calcium and magnesium sulfates as potential sources of sulfur dioxide during MSL SAM evolved gas analyses. In Proceedings of the Lunar and Planetary Science Conference, Houston, TX, USA, 13–17 March 2023.
12. Mahaffy, P.R.; Webster, C.R.; Cabane, M.; Conrad, P.G.; Coll, P.; Atreya, S.K.; Arvey, R.; Barciniak, M.; Benna, M.; Bleacher, L.; et al. The Sample Analysis at Mars Investigation and Instrument Suite. *Space Sci. Rev.* **2012**, *170*, 401–478. [CrossRef]
13. Sutter, B.; McAdam, A.C.; Mahaffy, P.R.; Ming, D.W.; Edgett, K.S.; Rampe, E.B.; Eigenbrode, J.L.; Franz, H.B.; Freissinet, C.; Grotzinger, J.P.; et al. Evolved gas analyses of sedimentary rocks and eolian sediment in Gale Crater, Mars: Results of the Curiosity rover's sample analysis at Mars instrument from Yellowknife Bay to the Namib Dune. *J. Geophys. Res. Planet.* **2017**, *122*, 2574–2609. [CrossRef]

14. Webster, C.R.; Mahaffy, P.R.; Atreya, S.K.; Flesch, G.J.; Farley, K.A. Measurements of Mars Methane at Gale Crater by the SAM Tunable Laser Spectrometer on the Curiosity Rover. In Proceedings of the Lunar and Planetary Science Conference, Houston, TX, USA, 13–17 March 2023.
15. Freissinet, C.; Glavin, D.P.; Mahaffy, P.R.; Miller, K.E.; Eigenbrode, J.L.; Summons, R.E.; Brunner, A.E.; Buch, A.; Szopa, C.; Archer, P.D.; et al. Organic molecules in the Sheepbed Mudstone, Gale Crater, Mars. *J. Geophys. Res. Planet.* **2015**, *120*, 495–514. [CrossRef]
16. Achilles, C.N.; Downs, R.T.; Ming, D.W.; Rampe, E.B.; Morris, R.V.; Treiman, A.H.; Morrison, S.M.; Blake, D.F.; Vaniman, D.T.; Ewing, R.C.; et al. Mineralogy of an active eolian sediment from the Namib dune, Gale crater, Mars. *J. Geophys. Res. Planet.* **2017**, *122*, 2344–2361. [CrossRef]
17. Rampe, E.B.; Bristow, T.F.; Morris, R.V.; Morrison, S.M.; Achilles, C.N.; Ming, D.W.; Vaniman, D.T.; Blake, D.F. Mineralogy of Vera Rubin Ridge from the Mars Science Laboratory CheMin Instrument. *J. Geophys. Res. Planets* **2020**, *125*, e2019JE006306. [CrossRef]
18. Rampe, E.B.; Lapotre, M.G.A.; Bristow, T.F.; Arvidson, R.E.; Morris, R.V.; Achilles, C.N.; Weitz, C.; Blake, D.F.; Ming, D.W.; Morrison, S.M.; et al. Sand Mineralogy Within the Bagnold Dunes, Gale Crater, as Observed In Situ and From Orbit. *Geophys. Res. Lett.* **2018**, *45*, 9488–9497. [CrossRef]
19. Achilles, C.N.; Rampe, E.B.; Downs, R.T.; Bristow, T.F.; Ming, D.W.; Morris, R.V.; Vaniman, D.T.; Blake, D.F.; Yen, A.S.; McAdam, A.C.; et al. Evidence for Multiple Diagenetic Episodes in Ancient Fluvial-Lacustrine Sedimentary Rocks in Gale Crater, Mars. *J. Geophys. Res. Planet.* **2020**, *125*, e2019JE006295. [CrossRef]
20. Fedo, C.M.; Bryk, A.B.; Edgar, L.A.; Bennett, K.A.; Fox, V.K.; Dietrich, W.E.; Banham, S.G.; Gupta, S.; Stack, K.M.; Williams, R.M.E.; et al. Geology and stratigraphic correlation of the Murray and Carolyn Shoemaker formations across the Glen Torridon region, Gale crater, Mars. *J. Geophys. Res. Planets* **2022**, *127*, e2022JE007408. [CrossRef]
21. Vaniman, D.T.; Bish, D.L.; Ming, D.W.; Bristow, T.F.; Morris, R.V.; Blake, D.F.; Chipera, S.J.; Morrison, S.M.; Treiman, A.H.; Rampe, E.B.; et al. Mineralogy of a Mudstone at Yellowknife Bay, Gale Crater, Mars. *Science* **2014**, *343*, 1243480. [CrossRef] [PubMed]
22. Treiman, A.H.; Bish, D.L.; Vaniman, D.T.; Chipera, S.J.; Blake, D.F.; Ming, D.W.; Morris, R.V.; Bristow, T.F.; Morrison, S.M.; Baker, M.B.; et al. Mineralogy, provenance, and diagenesis of a potassic basaltic sandstone on Mars: CheMin X-ray diffraction of the Windjana sample (Kimberley area, Gale Crater). *J. Geophys. Res. Planet.* **2016**, *121*, 75–106. [CrossRef] [PubMed]
23. Rampe, E.B.; Ming, D.W.; Blake, D.F.; Bristow, T.F.; Chipera, S.J.; Grotzinger, J.P.; Morris, R.V.; Morrison, S.M.; Vaniman, D.T.; Yen, A.S.; et al. Mineralogy of an ancient lacustrine mudstone succession from the Murray formation, Gale crater, Mars. *Earth Planet. Sci. Lett.* **2017**, *471*, 172–185. [CrossRef]
24. Yen, A.S.; Ming, D.W.; Vaniman, D.T.; Gellert, R.; Blake, D.F.; Morris, R.V.; Morrison, S.M.; Bristow, T.F.; Chipera, S.J.; Edgett, K.S.; et al. Multiple stages of aqueous alteration along fractures in mudstone and sandstone strata in Gale Crater, Mars. *Earth Planet. Sci. Lett.* **2017**, *471*, 186–198. [CrossRef]
25. Thorpe, M.T.; Bristow, T.F.; Rampe, E.B.; Tosca, N.J.; Grotzinger, J.; Bennett, K.A.; Achilles, C.N.; Blake, D.F.; Chipera, S.J.; Downs, G.W.; et al. Mars Science Laboratory CheMin Data From the Glen Torridon Region and the Significance of Lake-Groundwater Interactions in Interpreting Mineralogy and Sedimentary History. *J. Geophys. Res. Planets* **2022**, *127*, e2021JE007099. [CrossRef]
26. Berger, J.A.; Gellert, R.; Boyd, N.I.; King, P.L.; McCraig, M.A.; O'Connell-Cooper, C.D.; Schmidt, M.E.; Spray, J.G.; Thompson, L.M.; VanBommel, S.J.; et al. Elemental Composition and Chemical Evolution of Geologic Materials in Gale Crater, Mars: APXS Results From Bradbury Landing to the Vera Rubin Ridge. *J. Geophys. Res. Planets* **2020**, *125*, e2020JE006536. [CrossRef]
27. O'Connell-Cooper, C.D.; Thompson, L.M.; Spray, J.G.; Berger, J.A.; Gellert, R.; McCraig, M.; VanBommel, S.J.; Yen, A. Statistical Analysis of APXS-Derived Chemistry of the Clay-Bearing Glen Torridon Region and Mount Sharp Group, Gale Crater, Mars. *J. Geophys. Res. Planets* **2022**, *127*, e2021JE007177. [CrossRef]
28. Rapin, W.; Ehlmann, B.L.; Dromart, G.; Schieber, J.; Thomas, N.H.; Fischer, W.W.; Fox, V.K.; Stein, N.T.; Nachon, M.; Clark, B.C.; et al. An interval of high salinity in ancient Gale crater lake on Mars. *Nat. Geosci.* **2019**, *12*, 889–895. [CrossRef]
29. Fraeman, A.A.; Edgar, L.A.; Rampe, E.B.; Thompson, L.M.; Frydenvang, J.; Fedo, C.M.; Catalano, J.G.; Dietrich, W.E.; Gabriel, T.S.; Vasavada, A.R.; et al. Evidence for a Diagenetic Origin of Vera Rubin Ridge, Gale Crater, Mars: Summary and Synthesis of Curiosity's Exploration Campaign. *J. Geophys. Res. Planet.* **2020**, *125*, e2020JE006527. [CrossRef]
30. Glavin, D.P.; Freissinet, C.; Miller, K.E.; Eigenbrode, J.L.; Brunner, A.E.; Buch, A.; Sutter, B.; Archer, P.D.; Atreya, S.K.; Brinckerhoff, W.B.; et al. Evidence for perchlorates and the origin of chlorinated hydrocarbons detected by SAM at the Rocknest aeolian deposit in Gale Crater. *J. Geophys. Res. Planet.* **2013**, *118*, 1955–1973. [CrossRef]
31. Leshin, L.A.; Mahaffy, P.R.; Webster, C.R.; Cabane, M.; Coll, P.; Conrad, P.G.; Archer, P.D.; Atreya, S.K.; Brunner, A.E.; Buch, A.; et al. Volatile, Isotope, and Organic Analysis of Martian Fines with the Mars Curiosity Rover. *Science* **2013**, *341*, 1238937. [CrossRef] [PubMed]
32. Ming, D.W.; Archer, P.D.; Glavin, D.P.; Eigenbrode, J.L.; Franz, H.B.; Sutter, B.; Brunner, A.E.; Stern, J.C.; Freissinet, C.; McAdam, A.C.; et al. Volatile and Organic Compositions of Sedimentary Rocks in Yellowknife Bay, Gale Crater, Mars. *Science* **2014**, *343*, 1245267. [CrossRef]
33. McAdam, A.C.; Sutter, B.; Archer, P.D.; Franz, H.B.; Wong, G.M.; Lewis, J.M.T.; Clark, J.V.; Millan, M.; Williams, A.J.; Eigenbrode, J.L.; et al. Evolved gas analyses of sedimentary rocks from the Glen Torridon Clay-Bearing Unit, Gale crater, Mars: Results from the Mars Science Laboratory Sample Analysis at Mars Instrument Suite. *J. Geophys. Res. Planet.* **2022**, *127*, e2022JE007179. [CrossRef]

34. Sutter, B.; McAdam, A.C.; Wong, G.M.; Clark, J.V.; Archer, P.D.; Franz, H.B.; Gasda, P.J.; Ming, D.W.; Yen, A.; Lewis, J.M.T.; et al. Constraining Alteration Processes Along the Siccar Point Group Unconformity, Gale Crater, Mars: Results From the Sample Analysis at Mars Instrument. *J. Geophys. Res. Planets* **2022**, *127*, e2022JE007387. [CrossRef]
35. McAdam, A.C.; Sutter, B.; Archer, P.D.; Franz, H.B.; Wong, G.M.; Lewis, J.M.T.; Eigenbrode, J.L.; Stern, J.C.; Knudson, C.A.; Clark, J.V.; et al. Constraints on the Mineralogy and Geochemistry of Vera Rubin Ridge, Gale Crater, Mars, From Mars Science Laboratory Sample Analysis at Mars Evolved Gas Analyses. *J. Geophys. Res. Planet.* **2020**, *125*, e2019JE006309. [CrossRef]
36. Uchida, S.; Kamo, H. Reaction kinetics of formation of HCl in municipal refuse incinerators. *Ind. Eng. Chem. Proc. Dd* **1983**, *22*, 144–149. [CrossRef]
37. Stern, J.C.; Sutter, B.; Archer, P.D.; Eigenbrode, J.L.; McAdam, A.C.; Franz, H.B.; Knudson, C.; Ming, D.W.; Wong, G.; Freissinet, C.; et al. Major Volatiles Evolved From Eolian Materials in Gale Crater. *Geophys. Res. Lett.* **2018**, *45*, 10240–10248. [CrossRef]
38. Rapin, W.; Chauvire, B.; Gabriel, S.J.; McAdam, A.; Ehlmann, B.L.; Hardgrove, C.; Meslin, P.-Y.; Rondeau, B.; Dehouck, E.; Franz, H.; et al. In Situ Analysis of Opal in Gale Crater, Mars. *J. Geophys. Res. Planets* **2018**, *123*, 1955–1972. [CrossRef]
39. Zhang, P.; Cheng, J.; Jin, Y.; An, X. Evaluation of thermal physical properties of molten nitrate salts with low melting temperature. *Sol. Energy Mater. Sol. Cells* **2018**, *176*, 36–41. [CrossRef]
40. Olivares, R.; Chen, C.; Wright, S. The Thermal Stability of Molten Lithium–Sodium–Potassium Carbonate and the Influence of Additives on the Melting Point. *J. Sol. Energy Eng.* **2012**, *134*, 041002. [CrossRef]
41. Pavia, D.L.; Lampman, G.M.; Kritz, G.S. *Introduction to Organic Laboratory Techniques: A Contemporary Approach*; Saunders College Publishing: Philadephia, PA, USA, 1982.
42. Henriksson, M.; Warnqvist, B. Kinetics of Formation of Hcl(G) by the Reaction between Nacl(S) and So_2, O_2, and H_2O(G). *Ind. Eng. Chem. Proc. Dd* **1979**, *18*, 249–254. [CrossRef]
43. Robinson, H. Improvements in the Manufacture of Sulphate of Soda. Patent No. 149,859, 21 April 1872.
44. Scheidema, M.N.; Taskinen, P. Decomposition Thermodynamics of Magnesium Sulfate. *Ind. Eng. Chem. Res.* **2011**, *50*, 9550–9556. [CrossRef]
45. McAdam, A.C.; Franz, H.B.; Sutter, B.; Archer, P.D.; Freissinet, C.; Eigenbrode, J.L.; Ming, D.W.; Atreya, S.K.; Bish, D.L.; Blake, D.F.; et al. Sulfur-bearing phases detected by evolved gas analysis of the Rocknest aeolian deposit, Gale Crater, Mars. *J. Geophys. Res. Planet.* **2014**, *119*, 373–393. [CrossRef]
46. Yan, Z.; Wang, Z.; Liu, H.; Tu, Y.; Yang, W.; Zeng, H.; Qiu, J. Decomposition and solid reactions of calcium sulfate doped with SiO2, Fe2O3 and Al2O3. *J. Appl. Anal. Pyrolysis* **2015**, *113*, 491–498. [CrossRef]
47. ESTA®Kieserit FINE. Available online: https://www.kpluss.com/en-us/our-business-products/agriculture/products/en-esta-kieserit-fein/ (accessed on 15 January 2024).
48. Aparecida, C.; Rocha, A.; Cordeiro, G.C.; Toledo Filho, R.D. Use of thermal analysis to determine the hydration products of oil well cement pastes containing NaCl and KCl. *J. Therm. Anal. Calorim.* **2015**, *122*, 1279–1288. [CrossRef]
49. Birks, N. *Investigation into the Role of Sodium Chloride Deposited on Oxide and Metal Substrates in the Initiation of Hot Corrosion*; University of Pittsburg: Pittsburgh, PA, USA, 1983.
50. Wiedemann, H.; Smykatz-Kloss, W. Thermal studies of thernardite. *Thermochim. Acta* **1981**, *50*, 17–29. [CrossRef]
51. Rowe, J.J.; Morey, G.W.; Silber, C.C. The ternary system K2SO4·MgSO4·CaSO4. *J. Inorg. Nucl. Chem.* **1967**, *29*, 925–942. [CrossRef]
52. Chou, I.; Sealll, R. Determination of epsomite-hexahydrite equilibria by the humidity-buffer technique at 0.1 MPa with implications for phase equilibria in the system $MgSO_4$-H_2O. *Astrobiology* **2004**, *3*, 619–630. [CrossRef]
53. Stein, N.T.; Grotzinger, J.P.; Schieber, J.; Mangold, N.; Hallet, B.; Newsom, H.; Stack, K.M.; Berger, J.A.; Thompson, L.; Sieback, K.L.; et al. Desiccation cracks provide evidence of lake drying on Mars, Sutton Island member, Murray formation, Gale Crater. *Geology* **2018**, *46*, 515–518. [CrossRef]
54. Bonny, S.; Jones, B. Microbes and mineral precipitation, Miette Hot Springs, Jasper National Park, AB, Canada. *Can. J. Earth Sci.* **2003**, *40*, 1483–1500. [CrossRef]
55. Sankaranarayanan, K.; Timofeeff, M.N.; Spathis, R.; Lowenstein, T.K.; Koji Lum, J. Ancient microbes from halite fluid inclusions: Optimized surface sterilization and DNA extraction. *PLoS ONE* **2011**, *6*, e20683. [CrossRef]
56. Douglas, S.; Yang, H. Mineral biosignatures in evaporites: Presence of rosickyite in an endoevaporitic microbial community from Death Valley. *Calif. Geol.* **2002**, *30*, 1075–1078. [CrossRef]
57. Fish, S.A.; Shepherd, T.J.; McGenity, T.J.; Grant, W.D. Recovery of 16S ribosomal RNA gene fragments from ancient halite. *Nature* **2002**, *417*, 432–436. [CrossRef]
58. Kminek, G.; Bada, J.L.; Pogliano, K.; Ward, J.F. Radiation-Dependent Limit for the Viability of Bacterial Spores in Halite Fluid Inclusions and on Mars. *Radiat. Res.* **2003**, *159*, 722–729. [CrossRef]
59. Pavlov, A.; Eigenbrode, J.; Glavin, D.; Floyd, M. Rapid degradation of the organic moleulesin martian surface rocks due to exposure to cosmic rays. Severe implicatiosn to the search of the "extinct" life on Mars. In Proceedings of the Lunar and Planetary Science Conference, Houston, TX, USA, 13–17 March 2023.

Disclaimer/Publisher's Note: The statements, opinions and data contained in all publications are solely those of the individual author(s) and contributor(s) and not of MDPI and/or the editor(s). MDPI and/or the editor(s) disclaim responsibility for any injury to people or property resulting from any ideas, methods, instructions or products referred to in the content.